# Refractive Index Measurement Based on Thin-Core Fiber In-Line Mach-Zehnder Interferometer and Differential Intensity Demodulation

Xun Cai, Pan Pan, Sijie Chen, Haoran Wang, and Hongyan Fu, *Member, IEEE*

***Abstract*—A compact and reliable thin-core fiber (TCF) based in-line Mach-Zehnder interferometric (MZI) sensor for refractive index (RI) measurement is proposed and experimentally demonstrated. A section of TCF is sandwiched between a multi-mode fiber (MMF) and a single-mode fiber (SMF) to form the sensing head. In addition, the use of the differential intensity demodulation method not only greatly reduces the system cost, but also solves the problem of power fluctuation in the RI interrogation system. Three samples with different sensing lengths have been made, and the maximum sensitivity of 59.9 dB/RIU has been obtained in the range of 1.332–1.411 RIU, which means the measurement resolution is about $1.669 \times 10^{-4}$ RIU. Besides, the proposed MZI-based RI sensor is less sensitive to temperature, thus the cross-sensitivity effect can be greatly weakened.**

***Index Terms*—Differential intensity demodulation, fiber optic sensor, in-line Mach-Zehnder interferometer, refractive index measurement.**

## I. Introduction

OVER the past decades, refractive index (RI) sensor plays an important role in biomedicine, heavy metal ions detection, food safety and so on [1], [2], [3]. Compared with traditional electrical or fluorescence-based RI sensors, fiber optic RI sensors have been extensively studied due to their unique merits, such as easy fabrication, low cost, light weight, electromagnetic immunity and compactness. To accurately detect the surrounding refractive index (SRI), several types of sensors with different structures have been proposed, like fiber Bragg grating (FBG) sensors [4], long-period fiber Bragg grating (LPFBG) sensors, partially etched chirped fiber Bragg grating (pECFBG) sensor [5], fiber surface plasmon resonance (SPR) sensor [6] and fiber interferometric sensors [7], [8], [9], [10].

Among these schemes, the fiber modal interferometer-based sensors have attracted more attention due to the advantages of easy manufacture and high sensitivity. Jiao et al. revealed an MZI based on core and cladding modes coupling with sensitivity of −18.1764 nm/RIU within a narrow measurement range from 1.3105 to 1.3517 RIU [11]. Yang et al. presented an SMF-EYDF-SMF structure to measure the SRI change with maximum sensitivity of −22.811 nm/RIU, however, in addition to the broadband light source, the system also uses a 980 nm laser diode, which increases the system cost and introduces an extra power fluctuation effects [12]. Wang et al. demonstrated a cascaded fiber tapered MZI, which enjoys sensitivity of 158.4 nm/RIU, but still possesses a narrow measurement range of 1.33∼1.3792 RIU [13]. Chen et al. reported an RI sensor based on a cascaded taper structure with sensitivity up to 3751 nm/RIU, but with inadequate mechanical strength [14]. However, the mentioned sensors above usually utilize the wavelength demodulation method rather than intensity demodulation for RI measurement, which usually faces problems such as poor demodulation accuracy and high cost. Besides, this method usually has a trade-off between sensitivity and measurement range, that is, enjoying high sensitivity means no wide measurement range and vice versa. However, intensity demodulation-based interferometric RI sensors are often susceptible to light source fluctuation and modal power distribution variation in fibers, which hinders their application prospects. In order to address these shortcomings and improve the system's performance, many schemes have been proposed, such as the self-calibrated method [15] and the spectral peak-valley difference method [16].

In this paper, we have demonstrated an in-line MZI sensor based on single mode-multi mode-thin core-single mode fiber (SMTS) structure to measure SRI. Compared with the conventional wavelength demodulation scheme and considering the practicability, the differential intensity demodulation method (DIDM) has been utilized to reduce the system cost and eliminate the influence of optical power fluctuation. Comprehensive experimental measurements have been carried out in terms of SRI, temperature and stability. The maximum SRI sensitivity is around 59.9 dB/RIU in the sensing range of 1.332∼1.411 RIU when utilizing 14 mm thin core fiber (TCF) as the sensing element. Besides, the temperature-induced cross-sensitivity effect is only $4.5 \times 10^{-4}$ dB/°C, which has little influence on the intensity change and can be ignored in the real application.

## II. Operational Principal and Fabrication

The schematic diagram of proposed SMTS structure MZI is illustrated in Fig. 1(a). A section of thin-core fiber is sandwiched

Manuscript received 6 October 2022; revised 2 December 2022; accepted 6 December 2022. Date of publication 12 December 2022; date of current version 19 December 2022. This work was supported by National Natural Science Foundation of China (NSFC) under Grant 61975167. *(Corresponding author: Hongyan Fu.)*

The authors are with the Department of Electronic Engineering, School of Electronic Science and Engineering (National Model Microelectronics College), Xiamen University, Xiamen 361005, China (e-mail: caixun@stu.xmu.edu.cn; panpan9807@163.com; 23120201150216@stu.xmu.edu.cn; 23120200156685@stu.xmu.edu.cn; fuhongyan@xmu.edu.cn).

Digital Object Identifier 10.1109/JPHOT.2022.3228248

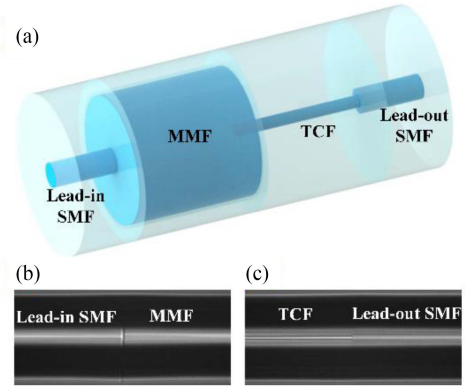


Fig. 1. (a) The schematic view of the proposed MZI based on SMTS structure; (b) and (c) are microscope images of the fabricated MZI near two ends, respectively.

between an MMF and a lead-out SMF to form the sensing head. As a mode coupler, the MMF excites many higher-order modes, which significantly enhances the power ratio between TCF's core and cladding modes. When the input light is emitted to the lead-in SMF and then passes through the MMF part, part of core mode power will couple into the excited cladding modes of TCF due to the mode field mismatch (MFM), while the rest of the core mode power will continue to propagate along the TCF. Due to the different propagation constants between core and cladding modes, the interference will occur at the TCF-SMF splicing point. All fibers are spliced with the Auto Mode splicing procedure (Fujikura, 66S) without any additional parameter setting. It should be noticed that although the splicing method is uncomplicated, careful cleaving is still required. Any unflatness of fiber end face will bring unnecessary loss for subsequent fiber fusion, and this fusion loss will affect the visibility of the transmission spectrum and insertion loss of the MZI.

In the process of fiber cleaving, a fiber cleaver (Fujikura, CT-08) with installed fiber clamp is required to increase the possibility of getting flat fiber end faces ($<2°$). To maintain the fiber perfectly level, the another end should also be carefully pulled by hand. The fabrication of the proposed RI sensor can be simply divided into the following three steps: firstly, the lead-in fiber SMF and MMF are spliced together to obtain SMF-MMF end, as shown in Fig. 1(b). Then, the TCF and the lead-out SMF are spliced together to obtain TCF-SMF end, as shown in Fig. 1(c). Finally, the two parts are spliced together to get the SMTS structure.

If the changes of mode polarization and mode field caused by environmental physical quantities are ignored, the transmission function of the MZI can be shown as follows [17]:

$$I = I_{co}(\lambda) + \sum_{m} I_{cl,m}(\lambda, n_{sur}) + 2\sum_{m} \sqrt{I_{co}(\lambda) \cdot I_{cl,m}(\lambda, n_{sur})} \cdot \cos\varphi \tag{1}$$

where $I_{co}(\lambda)$ and $I_{cl,m}(\lambda, n_{sur})$ represent the intensity of the core mode and mth order cladding modes, respectively. $\varphi = \frac{2\pi L}{\lambda}[n_{co}(\lambda) - n_{cl,m}(\lambda, n_{sur})]$ is the phase difference between core mode and cladding modes that produces the interference fringe in the transmission. $L$ is the length of sensing head. $n_{co}(\lambda)$, $n_{cl}(\lambda, n_{sur})$ and $\lambda$ are the core mode index, m-th cladding mode index and wavelength of the input light, respectively. $\Delta n = n_{co}(\lambda) - n_{cl,m}(\lambda, n_{sur})$ is the index difference between core and m-th cladding mode. Since the fiber core is not in contact with the external environment, its refractive index is thought to be almost unrelated with the surrounding refractive index. For $\varphi = (2k+1)\pi$, the m-th order destructive interference dip is given by :

$$\lambda = \frac{2\left[n_{co}(\lambda) - n_{cl,m}(\lambda, n_{sur})\right] \cdot L}{2k+1} \tag{2}$$

When the SRI increase continuously, the effective cladding mode index $n_{cl}(\lambda, n_{sur})$ will also increase correspondingly, which results in the blue shift of the transmission spectrum. The free spectrum range (FSR) of the transmission spectrum is determined by the optical path difference (OPD), $\Delta nL$ , as shown below:

$$FSR = \frac{\lambda^2}{\Delta nL} \tag{3}$$

Moreover, the intensity sensitivity $\frac{dI}{dSRI}$ of the MZI could be expressed as (4) by differentiating (1) with respect to SRI:

$$\frac{dI}{dSRI} = \frac{4\pi L}{\lambda} \sum_{m} \sqrt{I_{co}(\lambda) \cdot I_{cl,m}(\lambda, n_{sur})} \cdot \sin\left\{\frac{2\pi L}{\lambda}[n_{co}(\lambda) - n_{cl,m}(\lambda, n_{sur})]\right\} \times \frac{dn_{cl,m}(\lambda, n_{sur})}{dSRI} \tag{4}$$

From [18], we could know that the higher order cladding modes commonly have lower mode refractive indices and higher mode sensitivities $\frac{dn_{cl,m}(\lambda, n_{sur})}{dSRI}$. Because the higher the mode order is, the larger the mode field area will be, so it is more sensitive to external SRI. In addition, it can also be found that the intensity sensitivity of the sensor is proportional to the length of the sensing head.

## III. Simulation and Experimental Setup

The propagation of light in the MZI is simulated by using beam propagation method (BPM). Numerical solution of the propagation field distribution along the MZI has been generated using the fiber parameters listed in Table I, with input wavelength $\lambda = 1550$ nm. As shown in the Fig. 2, the reimaging points within the MMF are evident at a Z position around 8 mm and 10 mm. This result is similar to that in [19]. However, considering the cutting accuracy ($\pm 0.5$ mm) of fiber and the problem of insertion loss, the optimal length of MMF is about 10 mm. Furthermore, when the light is coupled from the MMF to the TCF section, the power of the core mode is reduced again. But, the majority of the power still remains in the fiber core due to the high numerical aperture (NA) of the TCF.

Fig. 3 shows the experimental setup of proposed SMTS structure in-line MZI based on TCF used for refractive index

TABLE I
FIBER PARAMETERS USED FOR SIMULATION

| Fiber Type | Core Diameter (μm) | Cladding Diameter (μm) | Core Index (RIU) | Cladding Index (RIU) | Length (μm) | NA |
|---|---|---|---|---|---|---|
| Lead-in and lead-out SMF(Corning ,28e) | 8.2 | 125 | 1.4514 | 1.4446 | 3000 | 0.14 |
| MMF(YOFC,SI 105) | 105 | 125 | 1.4523 | 1.4446 | 10700 | 0.15 |
| TCF(Nufern,UHNA7) | 2.4 | 125 | 1.501 | 1.4446 | 10000 | 0.41 |

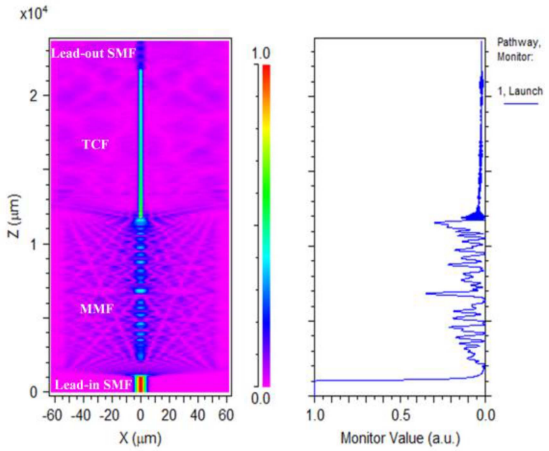


Fig. 2. Transmission field distribution and normalized output power along the MZI.

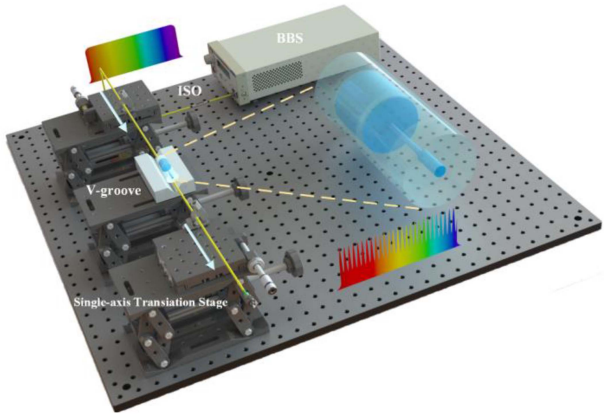


Fig. 3. Experimental setup of the RI sensor based on thin-core fiber in-line MZI.

measurement. A broadband light source (BBS) with the wavelength range of 1450∼1650 nm is coupled into the lead-in SMF after passing through an isolator (ISO). The interference spectrum is recorded by an optical spectrum analyzer (OSA) with resolution of 0.08 nm. To maintain straight lines and eliminate the bending loss, both ends of the sensor are fixed between two fiber fixtures, locked onto two single-axis translation stages. An unfixed V-groove is placed in the middle of the scissor-type lift platform (Zolix, MJ60), which has a lifting range of 60 mm.

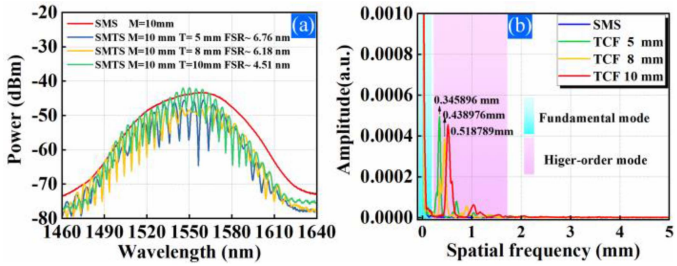


Fig. 4. (a) The transmission spectra of the fabricated SMTS structure with different lengths of TCFs in the air; (b) The corresponding spatial frequency spectra. M and T represent multi-mode and thin-core fiber, respectively.

To measure RI, the sensor head is immersed in various concentrations of glycerin aqueous solution. The refractive index of these glycerin aqueous solution varies from 1.332 to 1.411 RIU, which is corrected by a commercial refractometer with resolution of 0.001 RIU. Before each measurement, a disposable dropper was used to drop an aqueous glycerin solution into the V-groove. Due to the surface tension of the liquid, the solution will just soak the sensor head without flowing. After that, the sensing head is repeatedly rinsed with deionized water and alcohol until the spectrum is consistent with the original one in the air.

Fig. 4(a) shows the transmission spectrum of the fabricated SMTS structure with TCF lengths of 5, 8 and 10 mm. The transmission spectrum theoretically includes interference between the eigenmodes of the multimode fiber. But, there is no interference occurs when the length of TCF is 0 mm. The possible reason for this phenomenon is that the interference between the eigenmodes modes of the MMF core has a very large FSR, which is not within the measured output spectra [20]. The FSR of the SMTS structure decreases with the increase of sensing length L, which is consistence with (1). As shown in Fig. 4(b), the fast Fourier transform (FFT) spectra of the measured transmission spectra are also performed. There is only one main peak representing the fundamental mode in its spatial frequency spectrum when the TCF is 0 mm. As the length of TCF increases, the spatial frequency spectra of the MZIs exhibit bimodal characteristics due to the excitation of higher-order cladding modes. In addition, with the decrease of FSR, the spatial frequency gradually increases, which is consistent with the FFT theory. In our experiment, we have also made several SMF-TCF-SMF (STS) structures before making

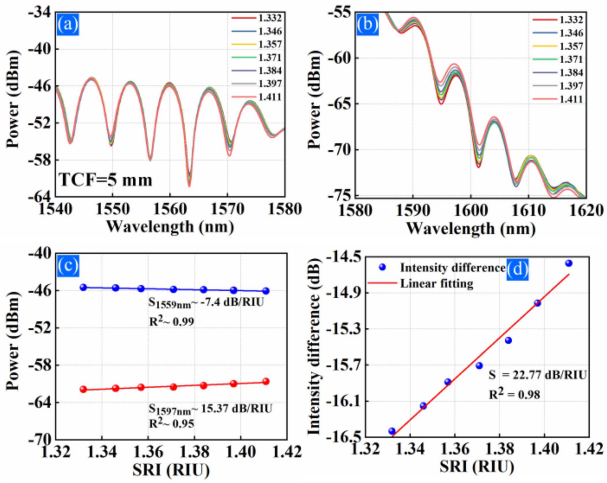


Fig. 5. Output spectra evolution of the proposed TCF based in-line MZI with different SRI when the length of TCF is 5 mm: (a) From 1540 nm to 1580 nm, (b) From 1580 nm to 1620 nm; The relationship between (c) intensity and (d) intensity difference of the chosen two wavelengths and the changing SRI.

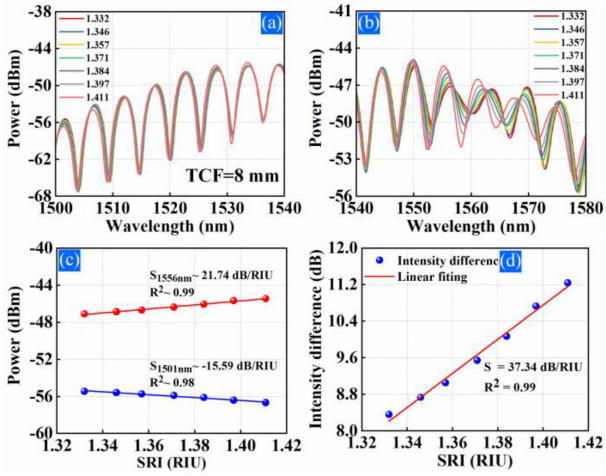


Fig. 6. Output spectra evolution of the proposed MZI with different SRI when TCF is 8 mm: (a) From 1500 nm to 1540 nm. (b) From 1540 nm to 1580 nm; The relationship between (c) intensity and (d) intensity difference of the chosen two wavelengths and the changing SRI.

SMTS structures. Although the insertion loss of STS structure is smaller than that of SMTS structure, its interference spectrum has some disadvantages such as low contrast, insignificant peak value and uneven range of free spectrum.

## IV. Results and Discussions

In our experiment, we have made three samples with different TCF lengths, and firstly investigated the RI sensing performance of the in-line MZI with 5 mm TCF at room temperature (25 °). During each measurement, the knob of the scissor-type lift table is rotated until the V-groove is aligned with the MZI as depicted in Fig. 3, which ensures that the sensing head is fully immersed in the glycerin solution. Fig. 5(a) and (b) reveal the transmission spectra evolution of the proposed TCF based in-line MZI with SRI varying from 1.332 to 1.411 within 40 nm spectral region. The linear relationship between the intensity of two chosen wavelengths (1559 nm, 1597 nm) and the RI variation is shown in Fig. 5(c). The intensity sensitivity of $\lambda_{1559\,\mathrm{nm}}$ is calculated to be $-7.4$ dB/RIU with good linearity of $R^2 = 0.99$ within the SRI range from 1.332 to 1.411 RIU, while for $\lambda_{1559\,\mathrm{nm}}$ , the proposed sensor exhibits the RI sensitivity of 15.37 dB/RIU. It is obvious that the transmission intensities at $\lambda_{1559\,\mathrm{nm}}$ and $\lambda_{1597\,\mathrm{nm}}$ change in the opposite trend with SRI. Therefore, SRI measurement can be achieved by monitoring changes in the intensity difference between the two wavelengths, and the differential intensity is more sensitive to SRI than either single wavelength. As shown in Fig. 5(d), the RI sensitivity of the proposed in-line MZI is improved to 22.77 dB/RIU after differential intensity demodulation, which also enjoys a good linearity of 0.98.

In addition, according to (4), the RI sensitivity is relevant to the length of the sensing head, so TCF with lengths of 8 mm and 10 mm are selected for the next experiments, respectively. The output spectra evolution of the in-line MZI sensor by using TCF with the length of 8 mm have been measured when the SRI changes from 1.332 to 1.411, as shown in Fig. 6(a) and (b). The chosen wavelengths used for demodulating the RI are 1501 nm and 1556 nm, labeled as $\lambda_{1501\,\mathrm{nm}}$ and $\lambda_{1556\,\mathrm{nm}}$. By comparing Fig. 6(a) and (b), it can be found that the phenomenon of spectral blue-shift after 1550 nm is more obvious, which may be caused by the fusion process. According to the Part II, the higher order cladding mode enjoys large mode sensitivity $\frac{dn_{cl,m}(\lambda,n_{sur})}{dSRI}$, which is more sensitive to the change of SRI. Thus, the change of SRI will lead to a greater change of the effective RI of the cladding mode, resulting in a smaller $\Delta n$. On the other hand, by observing the spatial frequency spectrum with TCF of 8 mm in Fig. 4(b), it can be found that the first dominant peak representing the higher order cladding mode is split, which generates more higher order modes to the interference process. From Fig. 6(c) and (d), the RI sensitivities of $\lambda_{1501\,\mathrm{nm}}$ and $\lambda_{1556\,\mathrm{nm}}$ by using TCF with length of 8 mm are estimated to be $-15.59$ dB/RIU and 21.74 dB/RIU, respectively. A higher RI sensitivity of 37.34 dB/RIU and linearity of 0.99 are obtained by the differential intensity demodulation.

To verify that the splicing process makes the blue-shift phenomenon more noticeable when TCF is 8 mm, another contrast experiment has been carried out with a TCF length of 10 mm. As shown in Fig. 7(a), only when the sensor head enters the low concentration glycerol solution ($n = 1.341$) from the air ($n = 1$) does the spectrum have a clear blue shift. Besides, the range of spectral movement with increasing RI is almost negligible when SRI changes from 1.341 to 1.411 RIU. Also, the chosen two wavelengths used to demodulate the SRI enjoy the intensity sensitivity of $-20.4$ dB/RIU and 22.18 dB/RIU, respectively. And the sensitivity of the TCF-based in-line MZI after differential intensity demodulation is up to 42.58 dB/RIU with good linearity of 0.997.

We have also conducted experiments with TCFs of 12 mm and 14 mm, respectively, to further illustrate the relationship between the sensor's sensitivity and the TCF's length, and the experimental results are displayed in Fig. 8. When TCF is 12 mm, the differential sensitivity is approximately 52.74 dB/RIU, whereas

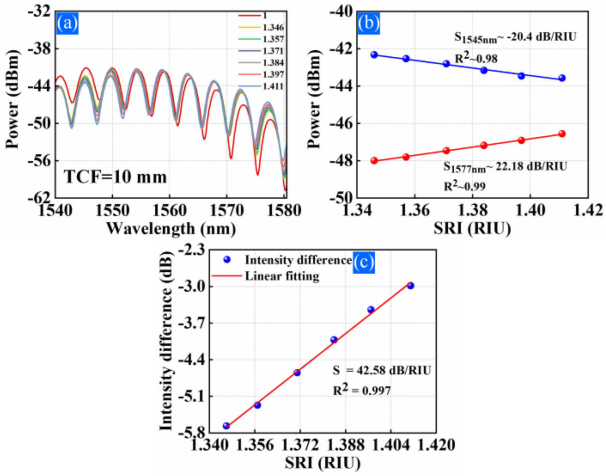


Fig. 7. (a) Output spectra evolution of the proposed MZI with different SRI when TCF is 10 mm from 1540 nm to 1580 nm. The relationship between (b) intensity and (c) intensity difference of two chosen wavelengths and the changing SRI.

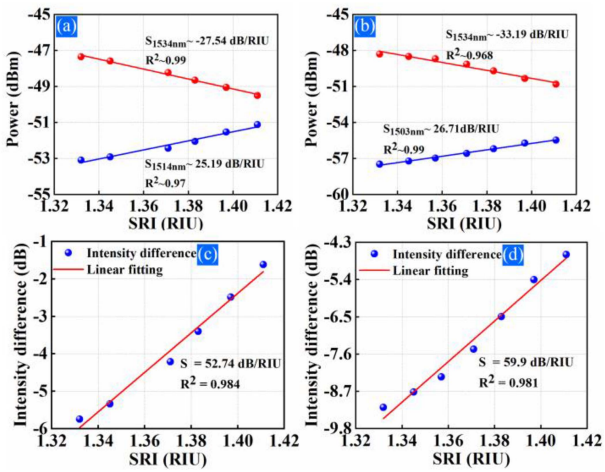


Fig. 8. The relationship between (a), (b) intensity and (c), (d) intensity difference of two chosen wavelengths and the changing SRI when TCF is 12/14 mm.

when TCF is 14 mm, the differential sensitivity increases to 59.9 dB/RIU, as can be observed by comparing Fig. 8(c) and (d). As a result, it can be said that the sensor's sensitivity is proportional to the length of the TCF, which is in accordance with the theoretical analysis.

Moreover, temperature change also has impacts on the RI measurement, which usually leads to the movement of the optical spectrum, resulting in crosstalk between temperature and refractive. In our experiment, the temperature characteristics of the in-line MZI sensor based on 14 mm TCF have been measured, and the sensing head was placed in a temperature control module (TCM) with the precision of ±0.01°C for temperature measurement. Fig. 9(a) displays the change of the transmission spectra in a wavelength range of 50 nm as temperature increases from 25 °C to 55 °C with a step of 5 °C, the optical spectrum experiences redshift with the increasing temperature. From Fig. 9(b), one can see that the temperature induced intensity sensitivities of the chosen wavelengths $\lambda_{1503\ nm}$ and $\lambda_{1534\ nm}$ are

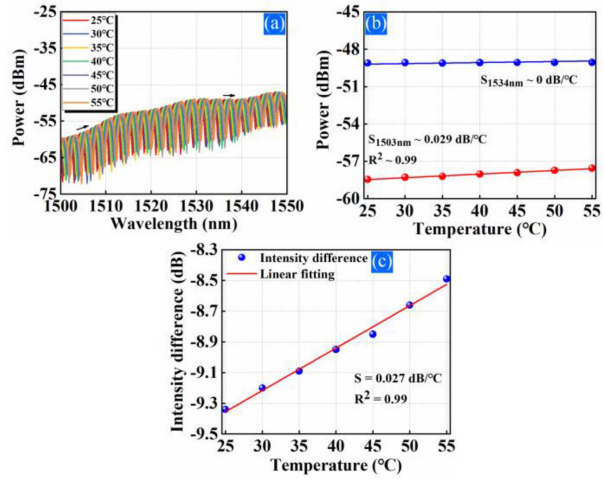


Fig. 9. (a) The measured output spectra of the 14 mm TCF-based in-line MZI sensor in the temperature range from 25 °C to 55 °C; The relationship between (b) intensity and (c) intensity difference of two chosen wavelengths and the temperature variation.

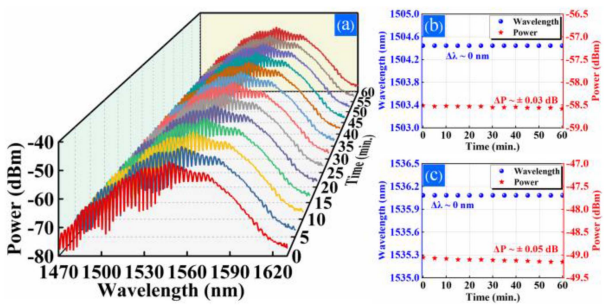


Fig. 10. (a) The repeated scanning spectra of the proposed TCF-based in-line MZI sensor in 60 minutes at n = 1; The wavelength and power stability of (b) 1504 nm and (c) 1536 nm at n = 1 in 1 hour with a step of 5 minutes.

estimated to be 0.029 dB/°C and nearly 0 dB/°C, respectively. Then, the maximum differential temperature sensitivity is only 0.027 dB/°C with good linearity of 0.99, as shown in Fig. 9(c). So, compared with the previous RI-induced intensity sensitivity, the temperature-induce one is much smaller, and the refractive index measurement error caused by the latter is about $4.5 \times 10^{-4}$ RIU/°C, which can be ignored in the practical application. Therefore, the RI sensing scheme based on differential intensity demodulation can effectively alleviate the cross-sensitivity problem.

Furthermore, the stability of the proposed RI sensor has been measured at 25/°C for 1 hour with n = 1, as depicted in Fig. 10. The wavelengths remain almost no shift and the intensity fluctuations are smaller than ±0.05 dB at both of chosen wavelengths for demodulating. After using the DIDM, the intensity difference ΔP is around ±0.03 dB, which means the corresponding refractive index measurement accuracy is $\pm 5.008 \times 10^{-4}$ RIU. The characteristics comparison of our work with other studies based on intensity demodulation is summarized in Table II [21], [22], [23], [24]. The most significant advantage of the proposed sensor is that it guarantees high sensitivity as well as a wide dynamic range, and is not affected by the fluctuations of the light source, which is mainly attributed to

TABLE II
COMPARISON OF CHARACTERISTICS WITH OTHER STUDIES

| Structures | Sensitivity (dB/RIU) | Dynamic range (RIU) | Power fluctuation resistance | Ref. |
|---|---|---|---|---|
| SMF-MMF MI | 94.58 | 0.0386 | No | 22 |
| SMF-tapered MMF-SMF MZI | 72.247 | 0.023 | No | 23 |
| Half-tapered SMS MZI | 345.78 | 0.015 | No | 24 |
| EFPI | 37 | 0.109 | No | 25 |
| SMTS MZI | 59.9 | 0.079 | Yes | This work |

***MI: modal interferometer, EPFI: extrinsic Fabry-Perot interferometer**

the differential intensity demodulation method. Considering the practical application, the sensor structure proposed in this paper can be configured with mature packaging technology, such as the packaging operation of a fiber fusion tapering machine.

## V. CONCLUSION

To sum up, we have demonstrated an RI sensor based on the in-line SMTS structure and differential intensity demodulation method. The sensor exhibits a maximum RI sensitivity of 59.9 dB/RIU from 1.332 to 1.411 RIU when the TCF is 14 mm. Furthermore, the temperature insensitivity and power fluctuation resistance of the proposed sensor will effectively solve the cross sensitivity problem between surrounding RI and temperature. The proposed RI sensor also enjoys the advantages of high RI sensitivity, broad measurement range, easy fabrication and cost-effectiveness, which makes it attractive for chemical and biological sensing applications.

## REFERENCES


[1] Z. Li et al., "Label-free detection of bovine serum albumin based on an in-fiber Mach-Zehnder interferometric biosensor," *Opt. Exp.*, vol. 25, no. 15, pp. 17105–17113, Jul. 2017.

[2] A. Celebanska et al., "Label-free cocaine aptasensor based on a long-period fiber grating," *Opt. Lett.*, vol. 44, no. 10, pp. 2482–2485, May 2019.

[3] A. Al Noman, J. N. Dash, X. Cheng, H.-Y. Tam, and C. Yu, "PCF based modal interferometer for lead ion detection," *Opt. Exp.,* vol. 30, no. 4, pp. 4895–4904, 2022.

[4] A. Iadicicco, A. Cusano, S. Campopiano, A. Cutolo, and M. Giordano, "Thinned fiber Bragg gratings as refractive index sensors," *IEEE Sensors J.,* vol. 5, no. 6, pp. 1288–1295, Dec. 2005.

[5] S. Korganbayev et al., "Partially etched chirped fiber Bragg grating (pECFBG) for joint temperature, thermal profile, and refractive index detection," *Opt. Exp.,* vol. 26, no. 14, pp. 18708–18720, Jul. 2018.

[6] M. D. C. Alonso-Murias, J. S. Velazquez-Gonzalez, and D. Monzon-Hernandez, "SPR fiber tip sensor for the simultaneous measurement of refractive index, temperature, and level of a liquid," *J. Lightw. Technol.,* vol. 37, no. 18, pp. 4808–4814, Sep. 2019.

[7] Y. L. Tian, Q. Zhang, and M. Han, "Microfluidic refractive index sensor based on an all-silica in-line Fabry–Perot interferometer fabricated with microstructured fibers," *Opt. Exp.,* vol. 21, no. 5, pp. 6633–6639, 2013.

[8] L. Linjun, R. Guobin, Y. Bin, P. Wanjin, L. Xiao, and J. Shuisheng, "Refractive index and temperature sensor based on fiber ring laser with STCS fiber structure," *IEEE Photon. Technol. Lett.,* vol. 26, no. 21, pp. 2201–2204, Nov. 2014.

[9] P. Chen, X. Shu, and K. Sugden, "Ultra-compact all-in-fiber-core Mach-Zehnder interferometer," *Opt. Lett.*, vol. 42, no. 20, pp. 4059–4062, Oct. 2017.

[10] H. Lu et al., "Temperature and liquid refractive index sensor using P-D fiber structure-based Sagnac loop," *Opt. Exp.,* vol. 26, no. 15, pp. 18920–18927, Jul. 2018.

[11] T. Jiao et al., "Simultaneous measurement of refractive index and temperature using a Mach-Zehnder interferometer with forward core-cladding-core recoupling," *Opt. Laser Technol.,* vol. 111, pp. 612–615, 2019.

[12] Z. Liu et al., "Sensitivity-Enhanced strain sensor based on thin-core fiber modal interferometer interacted with tilted fiber Bragg grating," *IEEE Sensors J.,* vol. 19, no. 5, pp. 1802–1806, Mar. 2019.

[13] Q. Wang, W. Wei, M. Guo, and Y. Zhao, "Optimization of cascaded fiber tapered Mach–Zehnder interferometer and refractive index sensing technology," *Sensors Actuators B: Chem.,* vol. 222, pp. 159–165, 2016.

[14] J. Chen, J. Zhou, Q. Zhang, H. Zhang, and M. - Y. Chen, "All-Fiber modal interferometer based on a joint-taper-joint fiber structure for refractive index sensing with high sensitivity," *IEEE Sensors J.,* vol. 13, no. 7, pp. 2780–2785, Jul. 2013.

[15] H. X. Wang, J. Wang, Z. Wang, W. Zhao, and R. G. May, "Self-calibrated interferometric–intensity-based optical fiber sensors," *J. Lightw. Technol.,* vol. 19, no. 10, pp. 1495–1501, Oct. 2001.

[16] L. C. B. Silva, L. B. Scandian, M. E. V. Segatto, and S. C. Ce, "Optical spectral intensity-based interrogation technique for liquid-level interferometric fiber sensors," *Appl. Opt.*, vol. 58, no. 35, pp. 9712–9717, Dec. 2019.

[17] E. H. Li, L. Chen, and X. Bao, "Application of spectrum differential integration method in an in-line fiber Mach-Zehnder refractive index sensor," *Opt. Exp.,* vol. 18, no. 8, pp. 8135–8143, 2010.

[18] T. Zhaobing and S. S. H. Yam, "In-Line single-mode optical fiber interferometric refractive index sensors," *J. Lightw. Technol.,* vol. 27, no. 13, pp. 2296–2306, Jul. 2009.

[19] Q. W. A. G. Farrell, "All-fiber multimode-interference-based refractometer sensor: Proposal and design," *Opt. Lett.*, vol. 31, no. 3, pp. 317–319, 2006.

[20] L. X. Li, Z. Xie, and D. Liu, "All-fiber Mach-Zehnder interferometers for sensing applications," *Opt. Exp.,* vol. 20, no. 100, 2012, Art. no. 11109.

[21] L. Hou, X. Zhang, J. Yang, J. Kang, and L. Ran, "Simultaneous measurement of refractive index and temperature based on half-tapered SMS fiber structure with fringe-visibility difference demodulation method," *Opt. Commun.,* vol. 433, pp. 252–255, 2019.

[22] Q. Sun, H. Luo, H. Luo, M. Lai, D. Liu, and L. Zhang, "Multimode microfiber interferometer for dual-parameters sensing assisted by Fresnel reflection," *Opt. Exp.*, vol. 23, no. 10, pp. 12777–12783, May 2015.

[23] H. Xue, H. Meng, W. Wang, R. Xiong, Q. Yao, and B. Huang, "Single-Mode-Multimode fiber structure based sensor for simultaneous measurement of refractive index and temperature," *IEEE Sensors J.,* vol. 13, no. 11, pp. 4220–4223, Nov. 2013.

[24] Y. J. R. Z. L. Ran, W. J. Liu, X. Liao, and K. S. Chiang, "Laser-micromachined Fabry-Perot optical fiber tip sensor for high-resolution temperatureindependent measurement of refractive index," *Opt. Exp.,* vol. 16, no. 3, pp. 2252–2263, 2008.